Optics Communications 282 (2009) 1374–1379

Contents lists available at ScienceDirect

Optics Communications

journal homepage: www.elsevier.com/locate/optcom

14-fs high temporal quality injector for ultra-high intensity laser

L. Antonucci [a,*], J.P. Rousseau [a], A. Jullien [a], B. Mercier [a], V. Laude [b], G. Cheriaux [a]

[a] Laboratoire d'Optique Appliquée, ENSTA ParisTech, Ecole Polytechnique, CNRS, Palaiseau, France
[b] Institut FEMTO-ST, Université de Franche-Comté, CNRS, ENSMM, UTBM, Besançon, France

ARTICLE INFO

Article history:
Received 9 September 2008
Received in revised form 12 December 2008
Accepted 12 December 2008

PACS:
42.65.Re
42.60.Jf
42.79.Wc

Keywords:
Ultra-fast pulse generation
High-contrast
Crossed polarized wave generation

ABSTRACT

We present a chirped pulse amplification (CPA) Ti:Sa laser generating sub-15 fs pulses with expected high temporal quality. Gain-narrowing in the pre-amplifier is balanced by a variable spectral reflectivity mirror and by a fine adaptation of the saturation conditions. A crossed polarized wave generation (XPW) filter is introduced to enhance the contrast, reduce the pulse duration and improve the spectral quality. The pulses are generated at 10 Hz repetition rate, with pulse energy of 110 μJ and very clean Gaussian spectrum. The temporal contrast is evaluated by a measurement before the XPW filter and calculations of the enhancement by the filter. The potential temporal incoherent contrast is 10^{12} and the coherent contrast 10^{10}. The performance of the system makes it suitable as an injector for petawatt lasers operating in the double-CPA scheme.

1. Introduction

Recently, much effort has been expended towards achieving ultra-high power lasers. In addition to increasing the energy, an important issue for many applications such as high-order harmonics generation and X-ray laser sources is to reduce the pulse duration to the sub-15 fs domain. For particle acceleration, although short pulse duration is not explicitly required, this feature enables one to reach dense plasma conditions with reduced energy. Another important topical research domain is the ultra-relativistic laser-matter interaction at intensities above 10^{22} W/cm^2 that are supplied by the new-generation petawatt (PW) lasers [1].

A critical characteristic of ultra-intense femtosecond pulses for most of the associated experiments is the temporal contrast, to prevent any modification of the target before the arrival of the main pulse, like pre-plasma formation. The temporal contrast includes coherent and incoherent contributions. A good coherent contrast is obtained by the compression of a Gaussian spectrum without any residual spectral phase. Residual high-order phase, spectral modulations or a super-Gaussian spectrum generally give rise to poor coherent contrast [2]. With regard to amplified spontaneous emission (ASE), the incoherent contrast of PW lasers has to be higher than 10^{11}. Consequently, an adequate pulse temporal quality involves both short duration and excellent coherent and incoherent contrast.

High-contrast in state-of-the-art high-intensity Ti:Sa femtosecond lasers is reached through temporal filtering, via different schemes. One solution is to supplement a classical CPA system [3] with a temporal filter (plasma mirrors) positioned after the compression stage [4]: the contrast can then be improved by four orders of magnitude but at the expense of 50% of the energy. Unfortunately, such losses can not be compensated for since the filter is the last element in the laser chain. Another solution is to insert a temporal filter before seeding the CPA laser, at the μJ energy level [5]. A third option is to use a double-CPA set-up including a temporal filter in between the two CPA systems, at the mJ energy level [6]. An advantage of this scheme is that the filtering effect occurs after the pre-amplifier, where most of the ASE is generated. Moreover, the energy losses introduced by the filter can be recovered by the subsequent power amplifiers. In particular, the suitability of nonlinear filters, based on cross-polarized wave (XPW) generation, for efficient ASE cleaning has already been demonstrated several times [5,7,8].

Regarding short pulse generation, pulses in the 10-fs regime with a Ti:Sa CPA system have been recently demonstrated though with poor peak-to-background contrast [9], while common high-contrast laser systems deliver pulses with durations exceeding several tens of femtoseconds. In view of short durations, optical parametric CPA (OPCPA) is also an interesting technique, since

* Corresponding author.
E-mail address: laura.antonucci@ensta.fr (L. Antonucci).

0030-4018/$ - see front matter © 2008 Elsevier B.V. All rights reserved.
doi:10.1016/j.optcom.2008.12.031

the spectral gain is relatively flat over a broad spectral bandwidth and sub-10 fs pulses can be generated and amplified [10]. Nevertheless, parametric fluorescence, analogously to ASE in Ti:Sa amplifiers, can reduce the incoherent contrast, while the coherent contrast is generally poor because of spectral modulations and phase distortions [11].

In this paper, we present a full study of an operational Ti:Sa injector for PW class lasers which offers both short pulse duration (sub-15 fs) and spectro-temporal quality. This front-end, including a pre-amplifier stage and a temporal filter, is designed to seed a PW laser in a double-CPA scheme. Besides contrast enhancement, the XPW temporal filter is here also employed as a pulse shortening device [12] and spectral shaper. The compression of 110 μJ pulses at 14 fs with quasi-Gaussian spectral distribution over more than 200 nm bandwidth is demonstrated. Previously validated models about XPW generation [13–16] allow us to expect 10^{12} incoherent contrast. The paper is organized as follows. We first present the experimental laser layout. Then, the employed methods to produce sub-15 fs pulses and the associated spatio-temporal effects are discussed. The last part of the paper focuses on temporal contrast characterization.

2. Experimental set-up

The proposed laser system takes advantage of the long knowledge of Ti:Sa amplification [17,18]. In particular, critical care is taken for the pulse temporal quality in the first amplification stage, where high gain usually results in a large amount of ASE and induces spectral narrowing. An advantage of the proposed system is the absence of active elements, often employed to limit spectral gain narrowing [19]. Solutions against gain narrowing without employing active devices are spectral filters in regenerative pre-amplifiers [9,20–23], or negatively and positively chirped pulse amplification in multi-pass pre-amplifiers [24].

Here, a spectral filter consisting of a specially designed mirror with variable spectral reflectivity (also termed gain-flattening mirror) is used to limit gain narrowing in a 10-pass pre-amplifier. Compared to a complex electronic device the reliability is increased, the alignment is straightforward, the injected energy is higher, and the cost is considerably reduced. The pre-amplification stage is followed by an optimized nonlinear filtering device relying on cross-polarized wave generation [13,25]. The XPW generation is a nonlinear phenomenon occurring in cubic crystals with anisotropic $\chi^{(3)}$ susceptibility, such as BaF_2 [14,26]. Its main benefits are an improvement of the temporal contrast and a reduction of the duration of the input pulse [8,27].

The experimental set-up is depicted in Fig. 1. The seed pulse is produced by a homemade ultra-broadband Ti:Sa oscillator based on Kerr lens mode-locking [28]. Group velocity dispersion (GVD) in the cavity of the Ti:Sa oscillator is compensated for by the use of negatively chirped mirrors and of a pair of fused silica prisms allowing a precise control of the spectrum. The prism pair generates a slightly positive GVD in order to shorten the distance between the prism apexes (separation of 28 cm) which makes the cavity less sensitive to beam pointing instability. The 4 mm long crystal is pumped by 3.5 W CW frequency doubled Nd:YVO4 laser (Verdi, Coherent). In this configuration, pulses with an energy of 4 nJ and a spectral bandwidth of 225 nm (centered at 804 nm) are produced.

The pulses are stretched in an Öffner type stretcher (0.7 ps/nm) consisting of a 1400 lines/mm diffraction grating (92% diffraction efficiency) and two spherical mirrors whose radii of curvature are 600 mm and 300 mm, respectively. Pulses at a repetition rate of 10 Hz are selected by a set of two high extinction ratio polarizers (10^5) and a KD*P Pockels cell.

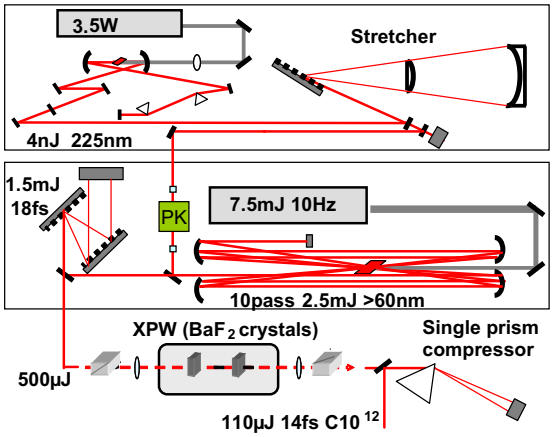

Fig. 1. Experimental set-up consisting of a large-band oscillator, an Öffner stretcher, a 10-pass pre-amplifier including a gain-flattening mirror, a grating compressor (20 fs), a XPW filter with improved efficiency thanks to the flat-top spatial shape of the injected beam and a single prism compressor (14 fs).

The stretched pulses are injected in a 10-pass pre-amplifier (configuration described in Ref. [29]) by using two pairs of co-focal concave mirrors (500 mm and 400 mm focal lengths). The variable reflectivity mirror (described in Section 3) is inserted after the fifth passage. The 6 mm long crystal is pumped by 7.5 mJ pulses at a repetition rate of 10 Hz with a highly super-Gaussian spatial beam profile (Surelite, Continuum), and the extracted energy is 2.5 mJ. Spatial filters are placed after the first, the fourth and the eighth passages for a fine adaptation of the infrared mode to the pump size. The amplification regime is highly saturated (1.8 J/cm^2). After the pre-amplifier, the pulse is compressed (20 fs) by a 1400 lines/mm gratings compressor presenting an overall efficiency of 50% and sent to the cross-polarized wave generation filter.

The XPW set-up is composed of two crossed polarizers, one focusing lens and one collimating lens, both with a 2000 mm focal length, and two BaF_2 crystals (crystallographic orientation [001], 2 mm thickness). The crystals are placed in a vacuum chamber (10^{-2} mbar) in order to avoid nonlinear effects in air. The distance between the two crystals is 25 cm and the first crystal is positioned 5 cm after the focal point. At this position the focusing systems images the amplifier output with a magnification factor of 0.5. The beam diameter is 1.8 mm at 13.5% of the maximum, leading to 500 μJ being injected into the filter to reach the optimal intensity (10^{12} W/cm^2) for conversion to orthogonal polarization. The conversion efficiency is 22% (loss-corrected from the uncoated faces of the crystals: 25%) and we were able to generate pulses of 110 μJ with a sub-15 fs duration.

3. Short pulse production

It is well-known that when the gain of an amplifier medium is not constant over the whole spectrum of the seed pulse, amplification tends to reduce the spectrum and to shift the central wavelength towards the gain maximum. This effect of spectral gain narrowing is dominant in the first amplifier of a Ti:Sa laser, since the gain is typically above 10^6. For this reason, even though seeding the amplifier with sub-10 fs pulses, it is difficult to amplify pulses shorter than 30 fs without special tricks. Another important effect happens when operating an amplifier above the saturation fluence: the leading edge of the pulse experiences a larger gain than the trailing edge. In the case of a positively dispersed pulse, like in a classical CPA, if the seeding spectrum is red-shifted compared to the gain maximum, the spectral gain tends to favor short wavelengths while saturation tends to mainly amplify long wavelengths.

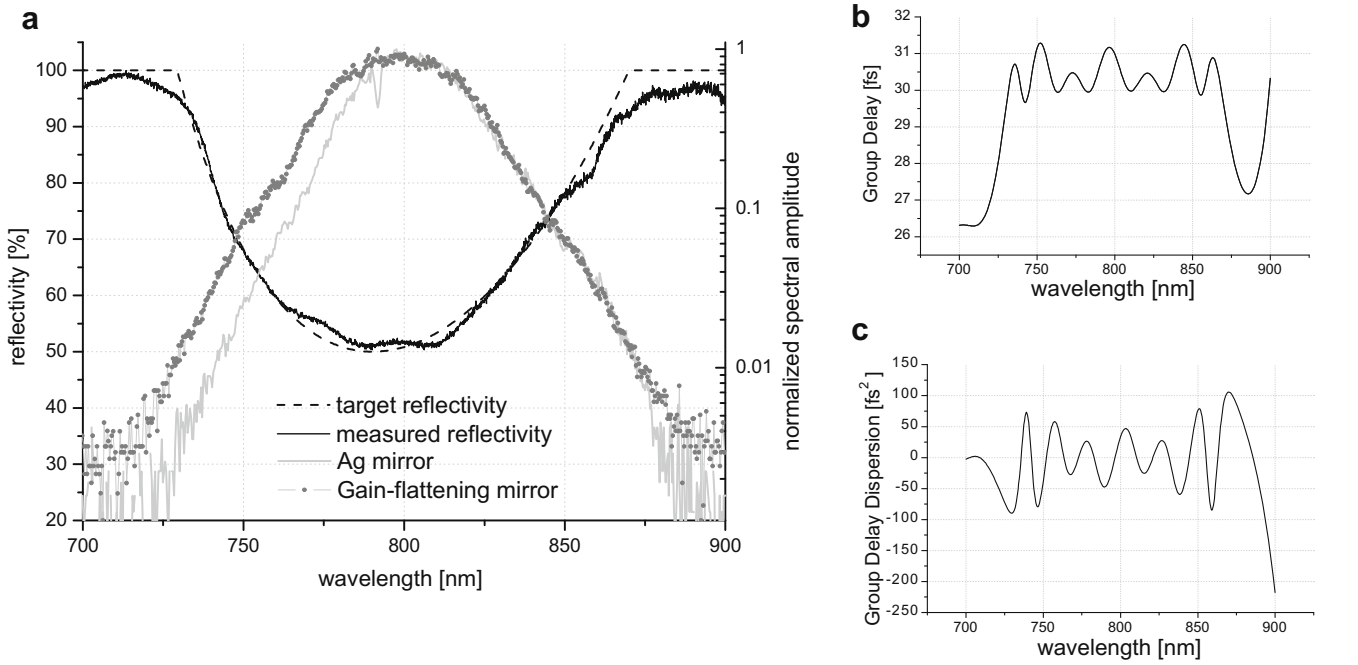

Fig. 2. Variable reflectivity mirror: (a) Target reflectivity (black dashed line) and measured reflectivity (black solid line) for the gain-flattening mirror design. Comparison of the amplified spectra with a silver mirror after the fifth passage (grey solid line) or with a gain-flattening mirror at the same position (grey dotted line). (b) Group delay. (c) Group delay dispersion.

Consequently, the two phenomena can partially compensate each other allowing the amplification of large spectra [30].

In our pre-amplifier, we reduced the spectral gain narrowing by a specifically designed mirror with variable spectral reflectivity. At the same time we injected a pulse that is spectrally centered at 804 nm for a gain maximum at 794 nm. We adjusted the saturation regime of the pre-amplifier to optimize the XPW filter operation. The result is high-contrast pulses production with almost 200 nm quasi-Gaussian spectral bandwidth.

3.1. Limiting gain narrowing: variable reflectivity mirrors

Gain-flattening mirrors were designed to compensate for spectral gain narrowing associated with amplification. The goal is to virtually flatten the gain curve by creating losses on the most amplified wavelengths, following a target spectral reflectivity (Fig. 2a), while exhibiting a very low group delay and GVD (Fig. 2b and c). The optimization procedure is to find a sequence of thin layers (and their thicknesses) reproducing as closely as possible the given target spectral reflectivity in amplitude and phase. Such a problem is similar to chirped mirrors optimization [31–33]. However, the spectral reflectivity target function has here a much stronger influence on the optimization process and the obtainable design, because the reflectivity is required to be 100% at both ends of the spectrum and varies smoothly to form a dip in the center. In contrast, a chirped mirror is normally intended to present a high reflectivity (e.g. 99.9% in the visible range) over a large bandwidth while providing at the same time for the prescribed dispersion. Chirped mirrors designed for femtosecond lasers in the visible and near-infrared spectral range are based on the alternation of two dielectric materials with high index contrast. The computation of the spectral reflectivity and phase of a stack of plane layers with complex refractive indices, i.e. including wavelength-dependent attenuation, can be performed with usual matrix methods [34] based on Maxwell's equations. Various optimization algorithms are also available. Here, we have used a Gibbs sampler optimization algorithm to obtain an optimal sequence of layer thicknesses, as described in reference [35]. The global error minimized by the algorithm is a linear weighted combination of a reflectivity criterion and of a phase criterion, as follows:

$$E = \alpha E[(R - R_0)^2] + \beta E[(t_g - t_{g0} - E[t_g - t_{g0}])^2] \quad (1)$$

where α and β are trade-off constants and $E(z) = \int_B d\omega z(w) / \int_B d\omega$ is the mean value of the function z over the target bandwidth B. In this equation, R is the reflectivity of the mirror under optimization and t_g is its group delay on reflection, while R_0 is the target reflectivity and t_{g0} is the target group delay.

Initial numerical experiments indicated that a strong index contrast is required for the variable reflectivity mirrors considered here, since the reflectivity on both edges of the spectral range should be close to unity. We chose to work with the silica (SiO_2) – tantalum oxide (Ta_2O_5) material system for its high index contrast and resistance to high power laser pulses. The wavelength dependence of the refraction index was precisely measured by ellipsometry and the experimental values included in the optimization program. We further observed that including a spectrally varying dispersion target in addition to the reflectivity target did not result in satisfying designs. Consequently, the target group delay variation was set to zero (no dispersion) in the final design. Reasonable convergence was obtained with 30 pairs of SiO_2 and Ta_2O_5 layers. The optimized result is shown in Fig. 2. The residual group delay and group delay dispersion do not affect the pulse duration: the temporal increase after one reflection is calculated to be lower than 0.1 fs, which is negligible compared to the effect of other dispersive elements in the system.

One variable reflectivity mirror was introduced after the fifth passage on the 10-pass pre-amplifier. In Fig. 2a, the grey dotted line curve and the grey solid line curve represent the amplified spectra using either the gain-flattening mirror or a common silver mirror. It is clear that in the first case a larger spectrum (44 nm instead of 37 nm FWHM) can be amplified and consequently a shorter pulse is produced. The two spectra have been obtained with a non-saturated amplification, in order to separate the influence of

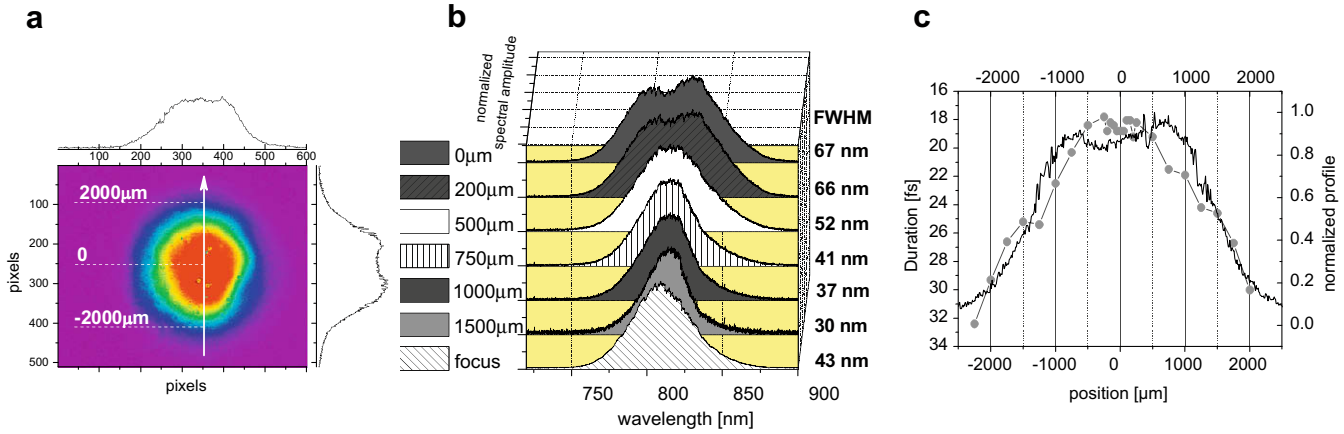

Fig. 3. Saturation effects. (a) Quasi flat-top spatial profile of the IR beam at the exit of the pre-amplifier. (b) Measurements of the spectrum at different positions along the vertical axis. (c) Evolution of the pulse duration (grey dotted line) along the vertical axis (black solid line).

the gain-flattening mirror from the saturation effects that will be presented afterwards.

3.2. Saturation: spectral and spatial beam shaping

As previously mentioned, the saturation phenomenon can help amplify large spectra when the central wavelength of the input pulse is red-shifted compared to the gain maximum like in our case. Another effect of the saturation concerns the spatial shape of the output beam that reproduces the super-Gaussian spatial profile of the pump beam (Fig. 3a).

Spectra of more than 60 nm FWHM have been measured after the pre-amplifier. Nevertheless, performing a spectrum measurement at different points of the spot beam, we noticed that saturation creates a spatial inhomogeneity in the spectral distribution. In Fig. 3b, we have reported the spectra measured along the vertical axis of the profile in the near-field, after amplification (Fig. 3a). It is worth pointing out that the spectra in the center of the spot are broader than at the sides. In Fig. 3c, the grey curve depicts the duration estimated by performing a FFT of each spectrum as a function of the spatial position: as expected, the pulse duration is shorter in the center (the minimum calculated duration is 17.8 fs). Moreover, the values of the duration and the values of the spatial intensity as functions of the position in the spot show essentially the same variations. This can be intuitively understood by the fact that saturation depends on the spatial intensity. Consequently, each point in the beam experiences a different degree of saturation producing a different amplification of long wavelengths as compared to short ones. We emphasize that the same experience was repeated in a non-saturated configuration and that no spatial inhomogeneity was observed in this case.

Further measurements were performed in the far field where the beam is focused. The resulting spectrum, identical in each part of the beam, is shown in Fig. 3b. The bandwidth is 44 nm FWHM and is comparable to the non-saturated case. Consequently, for immediate far-field applications, the advantage of the large bandwidth amplification due to saturation is canceled by spatial inhomogeneity and spectral averaging occurring at the focus. Nevertheless, interactions performed in the near or intermediate fields, like XPW filtering in our configuration, can benefit from the shortest duration at the central part of the beam.

3.3. Spatio-temporal characteristics of the XPW signal

In most cases the XPW filter is designed by positioning the first crystal at the beam waist, because of the good spatial beam quality at this position. In the present case the output of the pre-amplifier, almost top-hat shaped, is imaged in a plane after the focus, where the first BaF_2 crystal is positioned. This choice is motivated by three main reasons. First, the beam size enables us to seed the XPW filter with relatively high energy (500 µJ). Second, the conversion efficiency is increased as compared to a usual Gaussian shape [12]: while the common conversion efficiency for a Gaussian beam is around 15%, we converted 110 µJ from 500 µJ (25% internal efficiency) with a top-hat beam. Third, as previously underlined, the shortest duration is mapped in the spatial domain to the flat-top high intensity part of the beam. Since XPW generation depends on the cube of the input intensity, the shortest part of the beam will be mainly converted. Consequently, the spectral distribution is spatially homogenized and one can obtain a shortest final duration than by filtering at the focus.

This is illustrated in Fig. 4 where the spectra measured along the vertical axis of the beam after XPW (Fig. 4a) and the associated collimated beam profile (Fig. 4b) are reported. The homogeneity is significantly improved and the spectral shape is smooth and nearly Gaussian over a bandwidth of more than 200 nm. This spectral improvement is a consequence of the temporal cleaning achieved by the XPW process: the pulse wings related to a modulated spectrum with a square shape are decreased compared to the peak. This feature is then translated into the spectral domain as a more Gaussian spectrum. In Fig. 4c, the XPW spectrum is compared to the largest spectrum of the input pulse (evaluated in the center of the beam in the crystal plane) The total bandwidth of the XPW spectrum is about 1.6 times broader than the total bandwidth of the input spectrum, and about 1.8 times broader than the one of the spectrum at the focal point.

For a proof-of-principle, the pulse was compressed with a single silica prism compressor [36] to compensate for phase dispersion accumulated through the crystals, vacuum window, lens and essentially the second polarizer. The system does not allow a full compensation and a third order residual phase is present. The SPIDER measurement gives a temporal duration of 14 fs (Fig. 4d) while the Fourier transformed limited duration is estimated to be 12 fs, which corresponds to a pulse shortening in accordance with the measured spectral broadening.

4. High temporal quality

The obtained short duration is combined with high temporal quality, as discussed in this section. The high dynamical third order cross-correlation curve, measured after the pre-amplifier, is

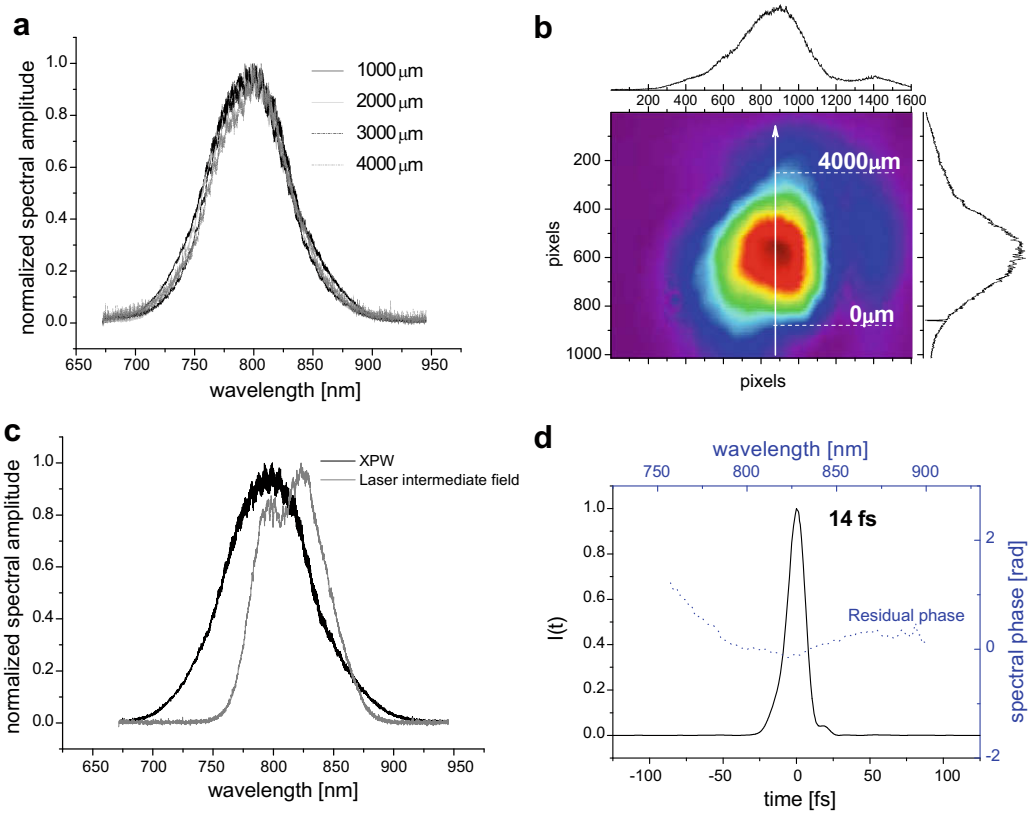

Fig. 4. XPW spectrum. (a) Measurements of the spectrum at different positions along the vertical profile of the beam after XPW. (b). Collimated beam profile after XPW. (c) Comparison between the laser spectrum at the intermediate field and the spectrum after XPW. The blue shift observed in the XPW signal is due to residual high order spectral phase [38]. (d) SPIDER measurement: XPW temporal intensity (left *y*-scale and low *x*-scale) and residual spectral phase (right *y*-scale and up *x*-scale).

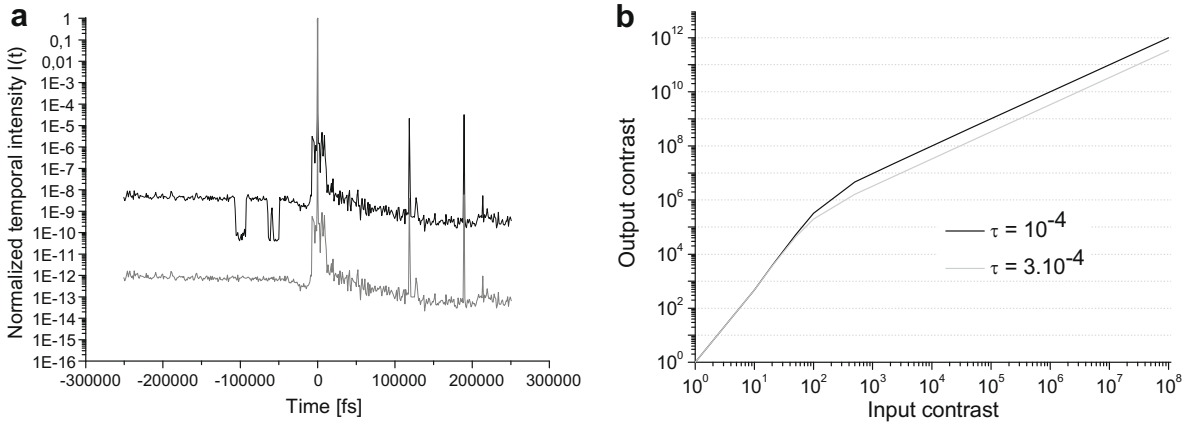

Fig. 5. Contrast: (a) third order cross-correlation curve measured after the pre-amplifier and the grating compressor (black line). Theoretical curve after XPW calculated with the experimental extinction ratio of the polarizing elements (grey line). (b) Evolution of the output contrast as a function of the input contrast for $\tau = 3 \times 10^{-4}$ and $\tau = 10^{-4}$.

depicted in Fig. 5. Despite the strong saturation regime, the contrast is kept at values that are common for pre-amplifiers: 10^8 for the incoherent contrast and 10^6 for the wings due to imperfect compression and spectral distortions. Regarding the incoherent contrast of the amplified beam, two reasons explain the good value that is obtained: first, the good matching between the pump mode and the seeding mode favors the amplification of the main pulse as compared to spontaneous emission; second, the gain-flattening mirror introduces losses on the ASE bandwidth and thereby limits its amplification.

The contrast measurement after the XPW filter is unrealizable for the energy level of 110 μJ at 10 Hz repetition rate. Nevertheless, it has already been demonstrated for this kind of filter that the ASE contrast enhancement is mainly limited by the extinction ratio between the two crossed polarizers [13].

We performed a theoretical calculation to estimate the potential improvement of coherent and incoherent contrast in our experimental scheme. The output signal $I_{out}(t)$ after filtering is composed of the XPW signal and the leakage of the input signal $I_{in}(t)$ through the crossed polarizers:

$$I_{out}(t) = I_{in}(t)(\eta(I_{in}(t))(1-\tau)+\tau) \quad (2)$$

where τ is the extinction ratio of the crossed polarizers and $\eta(I_{in}(t))$ is the conversion efficiency of the XPW process as a function of the intensity $I_{in}(t)$.The input and output contrasts are defined as:

$$C_{out}(t) = I_{outmax}/I_{out}(t) \quad (3)$$
$$C_{in}(t) = I_{inmax}/I_{in}(t) \quad (4)$$

I_{inmax}(resp. I_{outmax}) is the maximum input (resp. output) intensity.

The output contrast is deduced from (2):

$$C_{out}(t) = C_{in}(t)\eta_{max}/(\eta(I_{in}(t)) + \tau) \quad (5)$$

with η_{max}, the conversion efficiency for the maximum input intensity (at the peak of the pulse, $\eta_{max} = I_{outmax}/I_{inmax}$). We have $\tau \ll 1$ and $\eta_{max} \approx 1$.

To evaluate $C_{out}(t)$, $\eta(I_{in}(t))$ can be determined by solving numerically the complete system of equations describing the XPW process [15,16]. In the temporal region of interest (ASE and temporal wings) $I_{in}(t)$ is low ($<10^{-6} I_{inmax}$). For this low intensity regime, as XPW generation is a third order nonlinear effect, $I_{out}(t)$ is proportional to the third power of $I_{in}(t)$ [14],

$$I_{out}(t) = kI_{in}(t)^3 = \gamma_2^2 L^2 (2/c\varepsilon_0 n)^2 I_{in}(t)^3 \quad (6)$$

with L the length of the crystal, n the index of refraction and $\gamma_2 = n_2 c\varepsilon_0 n\pi/\lambda\sigma/4\sin(4\beta)$. n_2 is the nonlinear index, σ the nonlinear anisotropy of the crystal and β the angle between the incident polarization and the crystallographic axis of the crystal.

Consequently, we have:

$$\eta(I_{in}(t)) = I_{out}(t)/I_{in}(t) = kI_{in}(t)^3/I_{in}(t) = kI_{in}(t)^2 = kI_{inmax}^2/C_{in}(t)^2 \quad (7)$$

From Eqs. (5) and (7) the output contrast is rewritten:

$$C_{out}(t) = C_{in}(t)^3\eta_{max}/(C_{in}(t)^2\tau + kI_{inmax}^2) \quad (8)$$

k depends on the nonlinear crystal characteristics (BaF_2, $\beta = 22.5°$, $\sigma = -1.2$, $n_2 = 2 \times 10^{-20}$ m^2/W, $L = 4$ mm), we have $k = 2.1 \times 10^{-32}$ m^4 W^{-2}.

In our experimental configuration, we estimate the intensity $I_{inmax} = 10^{12}$ W/cm^2. The measured extinction factor between the two crossed polarizers lies between 3×10^{-4} and 10^{-4}. In Fig. 5b is reported the evolution of $C_{out}(t)$ as a function of $C_{in}(t)$ for these two values of τ. One can see that for both ASE (10^8) and coherent temporal wings (10^6), the contrast enhancement is only limited by the polarizers extinction ratio: $C_{out} = C_{in}\eta_{max}/\tau$.

We have calculated the expected and potential contrast after XPW filtering for $\tau = 10^{-4}$ using the simplified expression and the numerical resolution of the complete set of equations. The two methods give the same result. The corresponding curve is depicted on Fig. 5a.

It leads us to conclude that the expected final incoherent contrast is 10^{12} and the coherent contrast is 10^{10}.

5. Conclusion

We have presented a full injector system designed for a PW level laser in a double-CPA configuration. The characteristics of the saturated pre-amplifier are optimized to seed the XPW temporal filter, which offers control of the ASE level, pulse duration and spectral quality. The characteristics that make the presented injector suitable for the PW application are: the sub-15 fs duration, for operation at ultra-high intensities, in conjunction with a very good spectral quality for a good coherent contrast; the expected 10^{12} incoherent contrast makes it possible to amplify the pulse up to the PW level, while retaining the ASE pedestal below the plasma threshold; finally the fact that all elements are passive assures robust operation, easy alignment and relative low cost.

A further challenge is to preserve the pulse temporal duration and quality in the second PW level CPA. Here the incoherent contrast is supposed to be essentially preserved, since the typical gain of power amplifiers is of a few orders of magnitude (10^3 at the most) [4]. Moreover, a DAZZLER [37] will be used to finely tune the compression and to consequently improve the coherent contrast. Regarding duration, most of gain narrowing has been avoided in the first CPA. Nevertheless, efforts must be done in the second CPA to preserve the sub-15 fs duration at least in the first power amplifiers, which increases the energy from 110 μJ to the multi-mJ level.

Acknowledgements

We acknowledge support from DGA-ENSTA (Project No. 03 60.00.074.00.470.75.01) in the study of gain-flattening mirrors and thank Yong Ho Cha for experimental contributions.

References

[1] G.A. Mourou, T. Tajima, S.V. Bulanov, Rev. Mod. Phys. 78 (2006) 309.
[2] V. Bagnoud, F. Salin, IEEE J. Sel. Top. Quant. Electron. 4 (1998) 445.
[3] A.D. Strickland, G. Mourou, Opt. Commun. 56 (1985) 219.
[4] C. Thaury, F. Quéré, J.P. Geindre, A. Levy, T. Ceccotti, P. Monot, M. Bougeard, F. Réau, P. d'Oliveira, P. Audebert, R. Marjoribanks, P. Martin, Nat. Phys. 3 (2007) 424.
[5] V. Chvykov, P. Rousseau, S. Reed, G. Kalinchenko, V. Yanovsky, Opt. Lett. 31 (2006) 1456.
[6] M.P. Kalashnikov, E. Risse, H. Schönnagel, W. Sandner, Opt. Lett. 30 (2005) 923.
[7] A. Jullien, O. Albert, F. Burgy, G. Hamoniaux, J.P. Rousseau, J.P. Chambaret, F. Augé-Rochereau, G. Chériaux, J. Etchepare, N. Minkovski, S.M. Saltiel, Opt. Lett. 30 (2005) 920.
[8] A. Cotel, A. Jullien, N. Forget, O. Albert, G. Chériaux, C. Le Blanc, Appl. Phys. B 83 (2006) 7.
[9] A.A. Eilanlou, Y. Nabekawa, K.L. Ishikawa, H. Takahashi, K. Midorikawa, Opt. Express 16 (17) (2008) 13431.
[10] N. Ishii, L. Turi, V.S. Yakovlev, T. Fuji, F. Krausz, A. Baltuska, R. Butkus, G. Veitas, V. Smilgevicius, R. Danielius, A. Piskarskas, Opt. Lett. 30 (2005) 567.
[11] F. Tavella, K. Schmid, N. Ishii, A. Marcinkevičius, L. Veisz, F. Krausz, Appl. Phys. B 81 (2005) 753.
[12] A. Jullien, J.P. Rousseau, B. Mercier, L. Antonucci, O. Albert, G. Chériaux, S. Kourtev, N. Minkovski, S.S. Saltiel, Opt. Lett. 33 (2008) 2353.
[13] A. Jullien, S. Kourtev, O. Albert, G. Chériaux, J. Etchepare, N. Minkovski, S.M. Saltiel, App. Phys. B 84 (2006) 409.
[14] N. Minkovski, G.I. Petrov, S.M. Saltiel, O. Albert, J. Etchepare, J. Opt. Soc. Am. B 21 (2004) 1659.
[15] A. Jullien, O. Albert, G. Chériaux, J. Etchepare, S. Kourtev, N. Minkovski, S.M. Saltiel, J. Opt. Soc. Am. B 22 (2005) 2635.
[16] L. Canova, S. Kourtev, N. Minkovski, A. Jullien, R. Lopez-Martens, O. Albert, S.M. Saltiel, Appl. Phys. Lett. 92 (2008) 231102.
[17] K.F. Wall, A. Sanchez, Lincoln Lab. J. 3 (1990) 447.
[18] C. Le Blanc, P. Curley, F. Salin, Opt. Commun. 131 (1996) 391.
[19] F. Verluise, V. Laude, Z. Cheng, C. Spielmann, P. Tournois, Opt. Lett. 25 (2000) 575.
[20] C.P.J. Barty, T. Guo, C. Le Blanc, F. Raksi, C. Rose-Petruck, J. Squier, K.R. Wilson, V.V. Yakovlev, K. Yamakawa, Opt. Lett. 21 (1996) 668.
[21] K. Yamakawa, C.P. Barty, Opt. Lett. 28 (2003) 2402.
[22] H. Takada, K. Torizuka, IEEE J. Sel. Top. Quant. Electron. 12 (2006) 201.
[23] H. Takada, M. Kakehata, K. Torizuka, Opt. Lett. 31 (2006) 1145.
[24] M.P. Kalashnikov, K. Osvay, I.M. Lachko, H. Schönnagel, W. Sandner, Appl. Phys. B 81 (2005) 1059.
[25] A. Jullien, O. Albert, G. Cheriaux, J. Etchepare, S. Kourtev, N. Minkovski, S.M. Saltiel, Opt. Express 14 (2006) 2760.
[26] D.C. Hutchings, J.S. Aitchison, J.M. Arnold, J. Opt. Soc. Am. B 14 (1997) 869.
[27] A. Jullien, L. Canova, O. Albert, D. Boschetto, L. Antonucci, Y.H. Cha, J.P. Rousseau, P. Chaudet, G. Cheriaux, J. Etchepare, S. Kourtev, N. Minkovski, S.M. Saltiel, Appl. Phys. B 87 (2007).
[28] Y.H. Cha, K.T. Lee, H.M. Park, J.M. Han, Y.J. Rhee, Laser J. Kor. Phys. Soc. 40 (2002) 250.
[29] P. Georges, F. Estable, F. Salin, J.P. Poizat, P. Grangier, A. Brun, Opt. Lett. 16 (1991) 144.
[30] Y.H. Cha, Y.I. Kang, C.H. Nam, J. Opt. Soc. Am. B 16 (1999) 1220.
[31] R. Szipöcs, K. Ferencz, Ch. Spielmann, F. Krausz, Opt. Lett. 19 (1994) 201.
[32] R. Szipöcs, A. Köhzi-Kis, Appl. Phys. B 65 (1997) 115.
[33] A.S. Morlens, P. Balcou, P. Zeitoun, C. Valentin, V. Laude, S. Kazamias, Opt. Lett. 30 (2005) 1554.
[34] F. Abeles, Ann. Phys. 5 (1950) 596–640. 706–782.
[35] S. Kirkpatrick, C.D. Gelatt Jr., M.P. Vecchi, Science 220 (1983) 671.
[36] S. Akturk, X. Gu, M. Kimmel, R. Trebino, Opt. Express 14 (2006) 10101.
[37] P. Tournois, Opt. Commun. 140 (1997) 245.
[38] L. Canova, O. Albert, N. Forget, B. Mercier, S. Kourtev, N. Minkovski, S.M. Saltiel, R. Lopez Martens, Appl. Phys. B (2008).